Image reconstruction via non-isotropic diffusion in Dubins/Reed–Shepp-like control systems.

Ugo Boscain, Jean-Paul Gauthier, Dario Prandi and Alexey Remizov

Abstract— We compare the image inpainting results of two models of geometry of vision obtained through control theoretic considerations (the semi-discrete versions of the Citti-Petitot-Sarti and Mumford Elastica models). The main feature described by these models is the lifting of 2D images to the 3D group of translations and discrete rotations on the plane $SE(2, N)$, done by the primary visual cortex. Corrupted images are then reconstructed by minimizing the energy necessary to activate neurons corresponding to the missing regions. This minimization procedure, which gives rise to Dubins/Reed–Shepp-like optimal control problems in the case of corrupted curves, is described by an hypoelliptic diffusion on $SE(2, N)$.

We present two numerical algorithms for the resolution of the diffusion equation in both models and then compare the results.

I. INTRODUCTION

In this paper we present image inpainting algorithms based on two models of the geometry of vision: the Citti-Petitot-Sarti (CPS) model [8], [14] and the Mumford Elastica (ME) model [13]. In particular, we improve on the semi-discrete approach introduced in [6] for the CPS model, and compare the image inpainting results obtained with the two models.

Assume that the grey levels of an image are given as a square-integrable function $f : \mathbb{R}^2 \to [0, 1]$.

The crucial neuro-physiological fact behind the models presented in this paper, is that the primary visual cortex V1 lifts the image from $\mathbb{R}^2$ to the bundle of directions of the plane $PT\mathbb{R}^2 = \mathbb{R}^2 \times P\mathbb{R}$. Indeed, with some simplifications, neurons of V1 are grouped into orientation columns. Each one of these columns is sensitive to visual stimuli at a given point of the retina $a \in \mathbb{R}^2$ for a given direction $v \in P\mathbb{R}$, independently of its orientation.

If the image is corrupted on a set $D \subset \mathbb{R}^2$, i.e., if f is defined only on $\mathbb{R}^2 \setminus D$, the inpainting of f in D is obtained by minimizing the cost representing the energy required to the visual cortex to excite orientation columns corresponding to points in D, and thus not directly excited by the image. Neuro-physiological evidence suggests that this cost is small

if the orientation column is near to already excited ones of similar direction.

When the image to be reconstructed is a curve, this gives rise to an optimal control problem that, depending on the choice of the cost, can be either of Reed–Shepp-like type (see e.g., [11], [18]) and defined on $PT\mathbb{R}^2$ in the case of the CPS model, or Dubins-like (see [1], [11], [16], [17]) and defined on the double cover of $PT\mathbb{R}^2$, the group of Euclidean motions $SE(2) = \mathbb{R}^2 \times \mathbb{S}^1$, in the case of the ME model. When the image is more complex, the reconstruction is obtained by applying the diffusion process naturally associated with these control affine systems. Indeed, from a stochastic point of view, one expects these diffusion process to follow (and thus reconstruct) the most probable missing curves.

Recently, in [6], based on various precedent contributions (see [12], [19]), the authors conjectured that indeed the visual cortex can detect only a finite number N of directions. This allows to replace $PT\mathbb{R}^2$ and $SE(2)$ with the group of translations and discrete rotations $SE(2, N) = \mathbb{Z}/N\mathbb{Z} \ltimes \mathbb{R}^2$, where the rotations are either of step π/N or $2\pi/N$, respectively. We remark that N needs not be large, indeed in the numerical results we used $N = 30$.

Concerning *how* the visual cortex lifts an image to $SE(2, N)$, it seems likely that this is done through multiple convolutions with orientation sensitive filters (like the Gabor filters), see e.g. [9]. In this paper, we will consider only a primitive version of this lift, where the lift $Lf : SE(2, N) \to \mathbb{R}$ of a function $f : \mathbb{R}^2 \to \mathbb{R}$ is defined as follows.

- For the CPS model: $(Lf)(x, y, r) = f(x, y)$ if $r\pi/N$ is the angle in $\{k\pi/N, k = 0, \ldots, N-1\}$ nearest to the direction (in $[0, \pi)$) of the level set of f passing through (x, y), otherwise $(Lf)(x, y, r) = 0$. If no level set is detected at (x, y), $Lf(x, y, r) = f(x, y)/N$ for any r.

- For the ME model: $(Lf)(x, y, r) = f(x, y)$ if $2r\pi/N$ or $2r\pi/N + \pi$ is the angle in $\{2k\pi/N, k = 0, \ldots, 2N-1\}$ nearest to the orientation (in $[0, 2\pi)$) of the level set of f passing through (x, y), otherwise $(Lf)(x, y, r) = 0$. If no level set is detected at (x, y), $Lf(x, y, r) = f(x, y)/2N$ for any r.

The main part of the paper is the presentation of the aforementioned models and of two algorithms for the numerical solution of the associated hypoelliptic diffusions. The first one, has been introduced in [6] and is based on non-commutative Fourier analysis and a standard finite-element spatial discretization on the image domain. The second one, which is the main contribution of this paper, is based on a

U. Boscain and A. Remizov are with Centre National de Recherche Scientifique (CNRS), CMAP, École Polytechnique, Route de Saclay, 91128 Palaiseau Cedex, France and Team GECO, INRIA-Centre de Recherche Saclay. `ugo.boscain@polytechnique.edu`, `alexey.remizov@cmap.polytechnique.fr`

J.-P. Gauthier and D. Prandi are with LSIS (Laboratoire des Sciences de l'Information et des Systèmes), Université de Toulon, Bat. R, BP 20132, 83957 LA GARDE CEDEX `gauthier@univ-tln.fr`, `prandi@univ-tln.fr`

periodic interpolation of the discrete input image, for which the evolution can be computed exactly.

In the last part of the paper, we present some inpainting results for the two models, obtained through these algorithms. We remark that no a priori knowledge on the shape or position of the corrupted area is required. Finally, we present some results obtained through an heuristic procedure introduced in [6] and called *dynamic restoration*. This procedure, exploiting knowledge of the corrupted parts, allows us to greatly improve our results.

The paper is structured as follows. In Section II, we present the optimal control problems associated with the two models. Then, in Section III, we define the hypoelliptic diffusions associated with these control systems. Sections IV and V are then devoted to describe the two algorithms used to compute the evolutions, while Section VI compares the image inpainting obtained through these algorithms. Finally, in Section VII we collect our concluding remarks.

II. CONTROL THEORETIC APPROACH

In this section we present the optimal control problems associated with the ME and the CPS models.

A. Curve reconstruction

Let $\gamma_0 : [a, b] \cup [c, d] \to \mathbb{R}^2$ be a smooth curve with missing data. We assume that $\gamma_0(b) \neq \gamma_0(c)$ and that the velocities $\dot{\gamma}_0(b)$ and $\dot{\gamma}_0(c)$ are well-defined and non-vanishing. Our aim is to find a curve $\gamma : [b, c] \to \mathbb{R}^2$ completing γ_0 and minimizing some cost. For γ to complete γ_0, we require that $\gamma(b) = \gamma_0(b)$ and $\gamma(c) = \gamma_0(c)$. Also, depending on the model, we will pose some conditions on the tangent vectors at the extremities.

In the ME model, the curve is reconstructed via Euler's elastica. Namely, we look for arc-length parametrized curves minimizing the energy-like cost

$$E_1(\gamma) = \int_0^{\text{length}(\gamma)} \left(1 + K_\gamma^2(s)\right) ds, \qquad (1)$$

Recall that, if $\gamma = (x, y)$, then $K_\gamma = \frac{\dot{x}\ddot{y} - \dot{y}\ddot{x}}{(\dot{x}^2 + \dot{y}^2)^{3/2}}$.

Such cost is well-defined for any $\gamma \in C^2$ parametrized by arc-length. For $v_1, v_2 \in \mathbb{R}^2$, let $v_1 \sim v_2$ if $v_1 = \alpha v_2$ for some $\alpha > 0$. It is classical (see e.g., [3], [15]) that cost (1) equipped with the initial conditions

$$\begin{cases} \gamma(b) = \gamma_0(b) \text{ and } \gamma(c) = \gamma_0(c), \\ \dot{\gamma}(b) \sim \dot{\gamma}_0(b) \text{ and } \dot{\gamma}(b) \sim \dot{\gamma}_0(b), \end{cases} \qquad (2)$$

admits minimizers on this set.

On the other hand, in the CPS model, the curve is reconstructed by fixing a time $T > 0$ and minimizing the energy-like cost

$$E_2(\gamma) = \int_0^T \left(\|\dot{\gamma}(t)\|^2 + \|\dot{\gamma}(t)\|^2 K_\gamma(t)^2\right) dt. \qquad (3)$$

For $v_1, v_2 \in \mathbb{R}^2$, let $v_1 \approx v_2$ if $v_1 = \alpha v_2$ for some $\alpha \neq 0$. Then, cost (3) admits minimizers when equipped with the

"projective" initial conditions

$$\begin{cases} \gamma(b) = \gamma_0(b) \text{ and } \gamma(c) = \gamma_0(c), \\ \dot{\gamma}(b) \approx \dot{\gamma}_0(b) \text{ and } \dot{\gamma}(b) \approx \dot{\gamma}_0(b). \end{cases} \qquad (4)$$

We remark that these minimizers, as opposed to the ones for cost (1), fail in general to be smooth since they admit cusps. See [5], where it is also proved the lack of existence of minimizers for cost (3) with initial conditions (2).

These costs, being small for short and straight curves, are good models for the energy required to excite inactivated neurons. However, the main reason of our interest is that they can be naturally interpreted as the quadratic costs associated with two control-affine systems, one on the space of the Euclidean motions $SE(2)$ and the other on the projectivized tangent bundle of the plane $PT\mathbb{R}^2$.

B. Lift in $SE(2)$ or in $PT\mathbb{R}^2$

Consider a smooth planar curve $\gamma : [b, c] \to \mathbb{R}^2$ with components (x, y). Then a natural lift of γ in $SE(2)$ is $L\gamma(t) = (x(t), y(t), \theta(t))$, where $\theta(t) \in \mathbb{R}/2\pi\mathbb{Z}$ represents the direction of $\dot{\gamma}(t)$ with respect to the vector $e_1 = (1, 0)$.

Let us define on $SE(2)$ the vector fields $X_1(x, y, \theta) = \cos\theta \partial_x + \sin\theta \partial_y$ and $X_2(x, y, \theta) = \partial_\theta$. Then, a curve $\tilde{\gamma} : [b, c] \to SE(2)$ is the lift of some arc-length parametrized curve γ on $\mathbb{R}^2$ with $\dot{\gamma} \neq 0$ if and only if $\dot{\tilde{\gamma}} = X_1(\tilde{\gamma}) + v(t)X_2(\tilde{\gamma})$ for some function $v : [b, c] \to \mathbb{R}$.

Mutans mutandis, it is clear how to define the lift of planar curves in $PT\mathbb{R}^2$, for which $SE(2)$ is a topological double cover. Since no confusion arise, to lighten the notation we will still denote the lift by $L\gamma$. Observe that the projection of the vector fields X_1 and X_2 on $PT\mathbb{R}^2$ is well defined. Hence, curves on $PT\mathbb{R}^2$ that are lifts of planar curves are characterized by $\dot{\tilde{\gamma}} = u_1(t)X_1(\tilde{\gamma}) + u_2(t)X_2(\tilde{\gamma})$, where $u = (u_1, u_2) : [b, c] \to \mathbb{R}^2$.

C. Associated control-affine problems

In the previous discussion, $v(t) = K_\gamma(t)$ while $u_1(t) = \|\dot{\gamma}(t)\|$ and $u_2(t) = \|\dot{\gamma}(t)\| K_\gamma(t)$. Thus, relaxing our research to absolutely continuous curves, we can translate the curve reconstruction problem in optimal control terms.

Namely, in the case of the ME model, we obtain the following free-time control-affine optimal control problem on $SE(2)$,

$$\begin{cases} (\dot{x}, \dot{y}, \dot{\theta}) = X_1(x, y, \theta) + vX_2(x, y, \theta), \\ \int_0^T (1 + v(t)^2) \, dt \longrightarrow \min, \\ T > 0, \\ (x(0), y(0), \theta(0)) = L\gamma(b), \\ (x(T), y(T), \theta(T)) = L\gamma(c). \end{cases} \qquad (5)$$

For the CPS model, on the other hand, we obtain the following nonholonomic optimal control problem on $PT\mathbb{R}^2$,

$$\begin{cases} (\dot{x}, \dot{y}, \dot{\theta}) = u_1(t)X_1(x, y, \theta) + u_2X_2(x, y, \theta), \\ \int_0^T (u_1(t)^2 + u_2(t)^2) \, dt \longrightarrow \min, \\ (x(0), y(0), \theta(0)) = L\gamma(b), \\ (x(T), y(T), \theta(T)) = L\gamma(c). \end{cases} \qquad (6)$$

Here, $T > 0$ is fixed.

We remark that, since the vector fields $X_1, X_2, [X_1, X_2] = \sin\theta\partial_x - \cos\theta\partial_y$ are linearly independent, both these control systems satisfy the Hörmander condition, weakly in the case of the ME model (see [4], [10]). In particular, due to this fact, the control system in (6) defines a controllable sub-Riemannian structure. Also the control system in (5) is controllable, as it can be proved by direct computations.

III. STOCHASTIC INTERPRETATION

In this section we detail how to extend the curve reconstruction models described previously to image inpainting models. Henceforth, we will consider images given as grayscale functions $f : \mathbb{R}^2 \to [0, 1]$. Moreover, following [6], we will assume the visual cortex to be able to detect only a finite number N of angles, and hence we will work on $SE(2, N) = \mathbb{Z}/N\mathbb{Z} \ltimes \mathbb{R}^2$.

The lifting procedure described in the introduction amounts, in the case of the CPS model, to lift each level curve of f as described in Section II-B. For the ME model, on the other hand, the lifting of Section II-B takes into account the direction of the curve while level curves have no privileged directions. That is why we chose the lifting procedure described in the introduction that simply lifts twice each level curve: once with one orientation and once with the opposite one. See [7] for a more detailed analysis of the lifting procedure.

Once the function has been lifted, in principle one could apply the algorithm for the reconstruction of corrupted curves to reconstruct the corrupted level sets of the image. Although this has been done, e.g., in [2], it is clear that this technique cannot be applied to image inpainting for all types of images and corruptions. Indeed, in general it is not clear how to connect non-corrupted parts of the same level set.

To avoid this problem we adopt a stochastic point of view, considering the hypoelliptic diffusion equations associated with the control systems introduced in the previous section. Heuristically, these diffusions process will follow the most probable missing curves, reconstructing them.

First of all, let us define a jump Markov process Θ_t on $\mathbb{Z}/N\mathbb{Z}$ as follows. We let the law of the time of the first jump to be exponentially distributed with parameter $\beta > 0$ and jump probability $\frac{1}{2}$ on either side. Then, we obtain a Poisson process, with the probability of k jumps before time $t > 0$ given by

$$P(k \text{ jumps in } [0, t]) = \frac{(\beta t)^k}{k!} e^{-\beta t}.$$

The infinitesimal generator of Θ_t is the matrix $\Lambda_N = (\lambda_{i,j})_{i,j=0}^{N-1}$, defined by $\lambda_{i,i\pm 1} = \frac{1}{2}\beta$, $\lambda_{i,i} = -\beta$ and all the others $\lambda_{i,j}$ equal to zero.

A. Citti-Petitot-Sarti model

This is the model considered in [6], to which we refer for additional details.

Let us consider the following stochastic process with jumps

$$dZ_t = \begin{pmatrix} \cos\Theta_t \\ \sin\Theta_t \end{pmatrix} dW_t.$$

Here, Θ_t is a jump process on $\mathbb{Z}/N\mathbb{Z}$ and W_t is a Wiener process on $\mathbb{R}^2$.

Then, the infinitesimal generator of the semi-group associated with the stochastic process (Z_t, Θ_t) acts on any $\psi : SE(2, N) \to \mathbb{C}$ as

$$\mathcal{L}_N\psi = \frac{1}{2}A_r^2\psi + (\Lambda_N\psi)_r.$$

Here, $(\Lambda_N\psi(x, y, r))_r = \frac{\beta}{2}(\psi(x, y, r-1) - 2\psi(x, y, r) + \psi(x, y, r+1))$ and $A_r = \cos\theta_r\partial_x + \sin\theta_r\partial_y$, where $\theta_r = \frac{\pi r}{N}$.

Thus, representing functions on $SE(2, N)$ as $\phi : \mathbb{R}^2 \to \mathbb{C}^N$ and letting $A = \text{diag}(A_r)$, the diffusion equation for the CPS model is

$$\frac{d\phi}{dt} = \frac{1}{2}A^2\phi + \Lambda_N\phi. \tag{7}$$

As proved in [6], when $N \to +\infty$, diffusion (7) converges towards the standard CPS model hypoelliptic diffusion evolution on $PT\mathbb{R}^2$

$$\frac{d\varphi}{dt} = \frac{1}{2}(\cos\theta\partial_x + \sin\theta\partial_y)^2\varphi + \frac{\beta}{2}\partial_\theta^2\varphi.$$

Here, $\varphi : PT\mathbb{R}^2 \to \mathbb{R}$. This diffusion equation, as detailed in [14], [7], is associated with the sub-Riemannian control system (6).

B. Mumford Elastica model

Consider the Poisson process Θ_t defined before, and consider the following Markov process, introduced in [13],

$$dX_t = \begin{pmatrix} \cos\Theta_t \\ \sin\Theta_t \end{pmatrix} dt.$$

Here, no Wiener process on $\mathbb{R}^2$ is considered.

Then, the infinitesimal generator of the semi-group associated with the stochastic process (X_t, Θ_t) acts on any $\psi : \mathbb{R}^2 \times \mathbb{Z}/N\mathbb{Z} \to \mathbb{C}$ as

$$\mathcal{L}_N\psi = A_r\psi + (\Lambda_N\psi)_r,$$

where A_r and Λ_N are defined in the previous sections. Observe that, due to the absence of white noise, we obtain a diffusion operator with drift.

The diffusion equation for the ME model is then

$$\frac{d\phi}{dt} = A\phi + \Lambda_N\phi, \tag{8}$$

for any function on $SE(2, N)$ represented as $\phi : \mathbb{R}^2 \to \mathbb{C}^N$.

Letting $N \to +\infty$, diffusion (8) converges towards the hypoelliptic diffusion on $SE(2)$

$$\frac{d\varphi}{dt} = (\cos\theta\partial_x + \sin\theta\partial_y)\varphi + \frac{\beta}{2}\partial_\theta^2\varphi,$$

which is associated with the control-affine system (5).

IV. Evolution through discretization

In [6] a numerical scheme for the resolution of the CPS model is presented. Such model is based on a spatial discretization of the diffusion equation. In this section we describe this scheme and apply it also to the ME model.

Let the input image f being given as an $M \times M$ table of real values between $[0,1]$. We consider $G \subset \mathbb{R}^2$ to be the $M \times M$ grid on the plane with discretization step $\Delta x = \Delta y = \sqrt{M}$, i.e., such that the mesh points are $x_k = (k-1)/\sqrt{M}$ and $y_l = (l-1)/\sqrt{M}$ for $k, l = 0, \ldots, M-1$. In the following, for any function ψ defined on $SE(2,N)$, we will denote $\psi_{k,l}^r = \psi(x_k, y_l, r)$.

To discretize equations (7) and (8), we replace the differential operators ∂_x and ∂_y appearing in the operators A_r by their finite element approximations

$$D_x \psi_{k,l}^r = \frac{\psi_{k+1,l}^r - \psi_{k-1,l}^r}{x_{k+1} - x_{k-1}} = \frac{\sqrt{M}}{2}(\psi_{k+1,l}^r - \psi_{k-1,l}^r),$$

$$D_y \psi_{k,l}^r = \frac{\psi_{k,l+1}^r - \psi_{k,l-1}^r}{y_{l+1} - y_{l-1}} = \frac{\sqrt{M}}{2}(\psi_{k,l+1}^r - \psi_{k,l-1}^r).$$

Then, the discretized version of A is $D = \text{diag}(\cos\theta_r D_x + \sin\theta_r D_y)$. Replacing D to A in equations (7) and (8), we obtain their discretized versions. The initial condition for these equations will be the discrete analogue of the function Lf on $SE(2,N)$ obtained by lifting the original image.

Let us denote by $\widehat{\psi}_{k,l}^r$ the discrete Fourier transform (DFT) of ψ w.r.t. the variables k, l. Then, a straightforward computation shows that $A\widehat{\psi}_{k,l}^r = i\sqrt{M}a_{k,l}^r\psi_{k,l}^r$, where

$$a_{k,l}^r = \cos\theta_r \sin\left(2\pi\frac{k-1}{M}\right) + \cos\theta_r \sin\left(2\pi\frac{l-1}{M}\right).$$

Hence, the diffusion equations (7) and (8) are mapped by the DFT in the completely decoupled systems of M^2 ordinary linear differential equations on $\mathbb{C}^N$, respectively,

$$\frac{d\widehat{\psi}_{k,l}}{dt} = \left(\Lambda_N - \frac{M}{2}\text{diag}_r(a_{k,l}^r)^2\right)\widehat{\psi}_{k,l},$$

$$\frac{d\widehat{\psi}_{k,l}}{dt} = \left(\Lambda_N + i\frac{M}{2}\text{diag}_r(a_{k,l}^r)\right)\widehat{\psi}_{k,l},$$

where $k, l = 0, \ldots, M-1$ and $\widehat{\psi}_{k,l} = (\widehat{\psi}_{k,l}^0, \ldots, \widehat{\psi}_{k,l}^{N-1})^*$.

These discretized equations can then be solved through any numerical scheme. We chose the Crank-Nicolson method, for its good convergence and stability properties. Let us remark that the operators appearing on the r.h.s. are periodic tridiagonal matrices, i.e. tridiagonal matrices with non-zero $(1,N)$ and $(N,1)$ elements. Thus, the linear system appearing at each step of the Crank-Nicolson method can be solved through the Thomas algorithm for periodic tridiagonal matrices, of computational cost $\mathcal{O}(N)$.

V. Evolution through periodic approximation

We now present a new algorithm for the resolution of the CPS and ME diffusions.

A. Diffusion on trigonometric polynomials

For a compact subset $\mathcal{K}$ of $\mathbb{R}^2$, let $SE(2,N,\mathcal{K})$ be the set of $\mathbb{C}^N$-valued trigonometric polynomials $Q(x,y)$ with components,

$$Q^r(x,y) = \sum_{(\lambda_k,\mu_l)\in\mathcal{K}} c_{k,l}^r e^{i(\lambda_k x + \mu_l y)}, \quad r = 0, \ldots, N-1. \tag{9}$$

Here, $c_{k,l}^r \in \mathbb{C}$. Then, the semi-discrete diffusions (7) and (8) can be restricted to $SE(2,N,\mathcal{K})$, where they split in the completely uncoupled systems of linear ordinary differential equations

$$\frac{dc_{k,l}}{dt} = -2\pi^2\text{diag}\left(\lambda_k\cos\theta_r + \mu_l\sin\theta_r\right)^2 c_{k,l} + \Lambda_N c_{k,l}, \tag{10}$$

$$\frac{dc_{k,l}}{dt} = i\pi\text{diag}\left(\lambda_k\cos\theta_r + \mu_l\sin\theta_r\right) c_{k,l} + \Lambda_N c_{k,l}, \tag{11}$$

where $c_{k,l}(t) = (c_{k,l}^0(t), \ldots, c_{k,l}^{N-1}(t))^*$. These systems are equipped with initial conditions $c_{k,l}(0) = c_{k,l}$ from (9).

For the numerical resolution of these equations, the same considerations made at the end of Section IV are valid.

Remark 1: By [6, Theorem 2], solving (10) or (11) for some couple (λ_k, μ_l) is equivalent to solve it for any rotated couple $R_r(\lambda_k, \mu_l)$, associated with $r \in \mathbb{Z}/N\mathbb{Z}$. Thus, if the set $\mathcal{K}$ is invariant with respect to rotations R_r, $r \in \mathbb{Z}/N\mathbb{Z}$, it is indeed sufficient to solve (10) or (11) for a slice of $\mathcal{K}$ whose orbit under the rotations cover the whole $\mathcal{K}$.

B. Periodic interpolation

Any almost-periodic function ψ on $SE(2,N)$ is the uniform limit of $\mathbb{C}^N$-valued trigonometric polynomials of the form (9). Moreover, being a Moore group (all its irreducible representations are finite-dimensional), $SE(2,N)$ is maximally almost periodic, and hence every continuous function on $SE(2,N)$ can be uniformly approximated by almost-periodic functions. This yields to observe that given a continuous function on $SE(2,N)$ we could uniformly approximate it by a trigonometric polynomial of the form (9) and then evolve this approximation using (10) or (11).

Unfortunately, due to our choice of lift operation, there is no hope for any lifted image to be continuous on $SE(2,N)$, and hence this idea cannot be realized. We now show how to avoid this problem, exploiting the fact that the images (and their lifts) are indeed discrete functions defined on some pixel mesh $G \subset \mathbb{R}^2$.

Let ψ be a scalar function defined on $\mathbb{Z}/N\mathbb{Z} \times G \subset SE(2,N)$, in particular ψ could be the discrete lift of an image. We will let, as before, $\psi_{k,l}^r = \psi(x_k, y_l, r)$ where (x_k, y_l) is an enumeration of G and $r = 0, \ldots, N-1$. Then, for any r, the discrete Fourier transform $\widehat{\psi}_{k,l}^r$ is defined on $(\lambda_k, \mu_l) \in \widehat{G}$, the Pontryagin dual grid of G. Finally, we define the polynomial $Q \in SE(2,N,\widehat{G})$ by

$$Q^r(x,y) = \sum_{(\lambda_k,\mu_l)\in\widehat{G}} \widehat{\psi}_{k,l}^r e^{2\pi i(x\lambda_k + y\mu_l)}. \tag{12}$$

By Pontryagin duality, Q coincides with ψ when evaluated on points of the grid G. This interpolation allows to evolve ψ *exactly* using the uncoupled systems (10) and (11).

C. Numerical implementation

Let us explain more in detail how to obtain the coefficients of the approximation (12) starting from an image f defined on a square compact grid G with the sides composed of M pixels.

Up to translating the image, we can assume G to be symmetric w.r.t. the origin. As before, we consider the points of the grid to be uniformly spaced by $\sqrt{M}$, and hence the points of the grid have coordinates

$$x_k = \frac{k}{\sqrt{M}} - \frac{M-1}{2\sqrt{M}} \text{ and } y_l = \frac{l}{\sqrt{M}} - \frac{M-1}{2\sqrt{M}}.$$

By standard considerations, it holds that $\widehat{G} = G$.

Remark 2: The interpolating polynomial obtained in (12) is periodic on $\mathbb{R}^2$. If, as it is customary, we consider G to be contained in some square $[0, M] \times [0, M]$ of the first quadrant, then due to Remark 1 solving the equation (10) or (11) on $\widehat{G}$ indeed solves it on the bigger grid $\mathcal{K}$ obtained as orbit of $\widehat{G}$ under the rotations R_r, $r \in \mathbb{Z}/N\mathbb{Z}$. Hence, in order to recover correctly the inpainted image, one should take the inverse Fourier transform of the whole $\mathcal{K}$ and cut it as to contain only one copy of the inpainted image. Assuming the grid G to be symmetric w.r.t. the origin allows to avoid this step, since the orbit $\mathcal{K}$ is almost entirely contained in the same square as $\widehat{G}$, and thus the information loss due to ignoring it is small.

The following proposition shows that, up to elementwise operations, the computation of the discrete Fourier transform in (12) can be reduced to the discrete Fourier transform of an $M \times M$ matrix, computable through the FFT algorithm.

Proposition 1: Let $f : G \to \mathbb{R}$. Then, for any $(x_r, y_s) \in G$, it holds

$$f(x_r, y_s) = \sum_{(\lambda_k, \mu_l) \in \widehat{G}} \widehat{f}(\lambda_k, \mu_l) e^{2\pi i (x_r \lambda_k + y_s \mu_l)}, \quad (13)$$

with

$$\widehat{f}(\lambda_k, \mu_l) = \frac{1}{M} e^{2\pi i \frac{M-1}{2M}(k+l)}$$
$$DFT_{r,s} \left(e^{-2\pi i \left(\frac{M-1}{2M}\right)^2} e^{\frac{2\pi i}{M}(r+s)} f(x_r, y_s) \right)(k, l).$$

Here, $DFT_{r,s}$ denotes the discrete Fourier transform of a function depending on r and s. Namely

$$DFT_{r,s}(g(r,s))(k,l) = \frac{1}{M} \sum_{r,s=0}^{M-1} g(r,s) e^{\frac{2\pi i}{M}(rk+sl)}.$$

Proof: By (13), the expressions for $(x_r, y_s) \in G$ and $(\lambda_k, \mu_l) \in \widehat{G}$, and straightforward computations, we obtain

$$e^{-\frac{2\pi i}{M}\left(\frac{M-1}{2}\right)^2} e^{\frac{2\pi i}{M}\left(\frac{M-1}{2}\right)(r+s)} f(x_r, y_s) =$$
$$\frac{1}{M} \sum_{k,l=0}^{M-1} a_{k,l} M e^{-\frac{2\pi i}{M}\left(\frac{M-1}{2}\right)(k+l)} e^{\frac{2\pi i}{M}(rk+sl)}.$$

Fig. 1. Original image.

Fig. 2. Corrupted image.

Fig. 3. CPS model, with the discretization (left) and periodic approximation (right) algorithms.

Fig. 4. ME model, with the discretization (left) and periodic approximation (right) algorithms.

Observe that $f \in L^2(G)$, with respect to the Haar measure on G. Then, by Pontryagin duality, taking the Fourier transform on both sides of the equation yields the statement. ∎

Remark that, to use the indexes (k, l) instead of (λ_k, μ_l) in the ODEs (10) and (11), it is necessary to make the change of variables $\lambda_k = k/M - (M-1)/2$ and $\mu_l = l/M - (M-1)/2$.

VI. NUMERICAL RESULTS

The numerical implementation has been done mainly in Python, with the numerical resolution of equations (10) and (11) being implemented as a FORTRAN routine, for performances reasons.

A. Comparison of the models and the algorithms

In Figures 3 and 4 we present four examples of inpainting of the corrupted image in Figure 2, obtained through a very simple corruption of Figure 1.
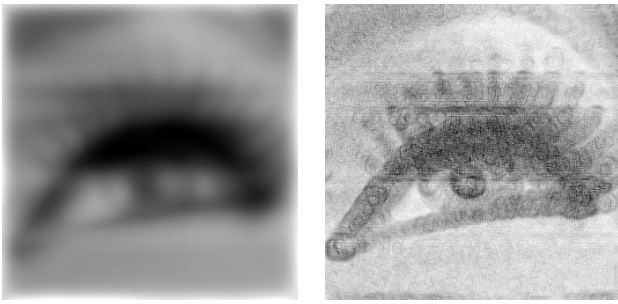
Fig. 5. CPS (left) and ME (right) models with long time of diffusion.

Fig. 6. Dynamic restoration with the CPS (left) and ME (right) models.

In particular, Figures 3(a) and 4(a) present the image inpainting results obtained using the discretization evolution scheme of Section IV, while Figures 3(b) and 4(b) present the image inpainting obtained from the periodic interpolation evolution scheme of Section V. Clearly, in all these examples the diffusions are applied for short time, to avoid an excessive action on the non-corrupted parts.

To better appreciate the purely diffusive nature of the CPS model as opposed to the presence of a transport term in the ME model, we present in Figure 5 two examples where the evolutions are applied on long time. Both these examples are obtained through the periodic interpolation algorithm.

B. Heuristic complements

The algorithms presented in this paper do not use any information on the corrupted area. In [6] an heuristic algorithm to improve on the results when information on the corrupted parts is available is presented. Without entering in the details, this procedure is based on mixing the evolved lifted image with the original lifted image where the image is not corrupted at given intervals of time. This can then be coupled with a technique to dynamically update the set of non-corrupted points, and the original image, allowing previously corrupted points to be considered non-corrupted when they become sufficiently similar to the neighboring pixels.

In Figure 6 we present two inpaintings obtained by applying this procedure to the periodic approximation algorithm.

VII. Conclusions

In this paper, we presented two models of geometry of vision with their control theoretic motivations, and their application to image inpainting via hypoelliptic diffusion. Moreover, we presented two algorithms to numerically compute this diffusion.

From the numerical experiments we did, the periodic approximation algorithm introduced in Section V of this paper, seem to be the more faithful and numerically stable. Once again, we would like to remark the fact that, except in Section VI-B, no information regarding the corruption has been used.

References

[1] A. A. Agrachev and Yu. L. Sachkov, *Control theory from the geometric viewpoint*, Encyclopaedia of Mathematical Science, vol. 87, Springer-Verlag, Berlin, 2004.

[2] A. Ardentov, A. Mashtakov, Yu. Sachkov, *Parallel Algorithm and Software for Image Inpainting via Sub-Riemannian Minimizers on the Group of Rototranslations*, Numer. Math. Theor. Meth. Appl., vol. 6 (2013), pp. 95–115.

[3] A. Ardentov, Yu. Sachkov, *Conjugate points in Euler's elastic problem*, JDCS, vol. 14 (2008), No. 3 (July), pp. 409–439.

[4] A. M. Bloch, *Nonholonomic Mechanics and Control*, Interdisciplinary Applied Mathematics, vol. 24, Springer-Verlag, Berlin, 2003.

[5] U. Boscain, G. Charlot, and F. Rossi, *Existence of planar curves minimizing length and curvature*, Proc. of the Steklov Institute of Mathematics, vol. 270 (2010), pp. 43–56.

[6] U. Boscain, R. Chertovskih, J.-P. Gauthier, and A. Remizov, *Hypoelliptic diffusion and human vision: a semi-discrete new twist*, SIAM J. Imaging Sci., vol. 7, No. 2 (2014), pp. 669–695.

[7] U. Boscain, J, Duplaix, J.-P. Gauthier, and F. Rossi, *Anthropomorphic image reconstruction via hypoelliptic diffusion*, SIAM J. Control Optim., vol. 50, No. 3 (2012), pp. 1309–1336.

[8] G. Citti, A. Sarti, *A cortical based model of perceptual completion in the roto-translation space*, J. Math. Imaging Vision, 2006, vol. 24 (3), pp. 307–326.

[9] J. G. Daugman, *Uncertainty relation for resolution in space, spatial frequency, and orientation optimized by two-dimensional visual cortical filters*, J. Optical Soc. America A, 1985, vol. 2 (7), pp. 1160–1169.

[10] F. Jean, G. Oriolo, and M. Vendittelli, *A globally convergent steering algorithm for regular nonholonomic systems*, In: 44th IEEE CDC-ECC'05, Seville, Spain, December 12-15, 2005.

[11] J.-P. Laumond (editor), *Robot motion planning and control*, Lecture Notes in Control and Information Science, vol. 229, Springer-Verlag London Ltd., London, 1998. Available online at: ftp.laas.fr/pub/ria/promotion/book.pdf

[12] T. S. Lee, *Image representation using 2D Gabor wavelets*, IEEE Trans. Pattern Anal. Machine Intel. 18 (1996), no. 10, pp. 959–971.

[13] D. Mumford, *Elastica and Computer Vision*, Algebraic Geometry and its Applications, Springer, New York, 1994, pp. 491–506.

[14] J. Petitot, *Neurogèométrie de la vision – Modèles mathématiques et physiques des architectures fonctionelles*, Les Éditions de l'École Polytechnique, 2008.

[15] Yu. Sachkov, *Maxwell strata in Euler's elastic problem*, JDCS, vol. 14, No. 2 (2008), pp. 169–234.

[16] M. Sigalotti, Y. Chitour, *Dubins' Problem on Surfaces II: Nonpositive Curvature*, SIAM J. Control and Optimization, 2006, vol. 45, No. 2, pp. 457–482.

[17] P. Souères, A. Balluchi, and A. Bicchi, *Optimal feedback control for route tracking with a bounded-curvature vehicle*, International Journal of Control, 2001, Vol. 74, No. 10, pp. 1009–1019.

[18] P. Souères and J.-P. Laumond, *Shortest paths synthesis for a car-like robot*, IEEE Trans. Automat. Control, 1996, vol. 41, No. 5, pp. 672–688.

[19] N. V. Swindale, D. Shoham, A. Grinvald, T. Bonhoeffer, M. Höbener, *Visual cortex maps are optimized for uniform coverage*, Nature Neuroscience, 2000, vol. 3, pp. 822–826.